Spectroscopic Characterization of Five- and Six-Coordinate Ferrous−NO Heme Complexes. Evidence for Heme Fe−Proximal Cysteinate Bond Cleavage in the Ferrous−NO Adducts of the Trp-409Tyr/Phe Proximal Environment Mutants of Neuronal Nitric Oxide Synthase[†]

Heather L. Voegtle,[‡] Masanori Sono,*,[‡] Subrata Adak,[§] Alycen E. Pond,[||] Takeshi Tomita,[⊥] Roshan Perera,[‡] David B. Goodin,[||] Masao Ikeda-Saito,[#] Dennis J. Stuehr,[§] and John H. Dawson*,[‡,▽]

Department of Chemistry and Biochemistry, University of South Carolina, 631 Sumter Street, Columbia, South Carolina 29208, Department of Immunology, Lerner Research Institute, Cleveland Clinic Foundation, 9500 Euclid Avenue, Cleveland, Ohio 44195, Department of Molecular Biology, The Scripps Research Institute, 10550 North Torrey Pines Road, La Jolla, California 92037, Department of Physiology and Biophysics, Case Western Reserve University School of Medicine, Cleveland, Ohio 44106-4970, and Institute of Multidisciplinary Research for Advanced Materials, Tohoku University, Katahira, Aoba, Sendai 980-8577, Japan

ABSTRACT: Nitric oxide synthases (NOS) are a family of cysteine thiolate-ligated heme-containing monooxygenases that catalyze the NADPH-dependent two-step conversion of L-arginine to NO and L-citrulline. During the catalysis, a portion of the NOS heme forms an inhibitory complex with self-generated NO that is subsequently reverted back to NO-free active enzyme under aerobic conditions, suggesting a downstream regulator role of NO. Recent studies revealed that mutation of a conserved proximal tryptophan-409, which forms one of three hydrogen bonds to the heme-coordinated cysteine thiolate, to tyrosine or phenylalanine considerably increases the turnover number of neuronal NOS (nNOS). To further understand these properties of nNOS on its active site structural level, we have examined the oxygenase (heme-containing) domain of the two mutants in close comparison with that of wild-type nNOS with UV−visible absorption, magnetic circular dichroism, and electron paramagnetic resonance spectroscopy. Among several oxidation and ligation states examined, only the ferrous−NO adducts of the two mutants exhibit spectra that are markedly distinct from those of parallel derivatives of the wild-type protein. The spectra of the ferrous−NO mutants are broadly similar to those of known five-coordinate ferrous−NO heme complexes, suggesting that these mutants are predominantly five coordinate in their ferrous−NO states. The present results are indicative of cleavage of the Fe−S bond in the nNOS mutants in their ferrous−NO state and imply a significant role of the conserved tryptophan in stabilization of the Fe−S bond.

Nitric oxide (NO)[1] has been shown to provide such physiologically important functions as a neurotransmitter, vasodilator, and cytotoxic agent (*1−8*). NO biosynthesis is dependent on a family of enzymes called NO synthases (NOS). Three isoforms of NOS have been characterized including neuronal (nNOS), macrophage (iNOS), and endothelial (eNOS) enzymes. NOS catalyzes the NADPH-dependent oxidation of L-arginine (L-Arg) by O_2 with the formation of L-citrulline and NO in two steps. The first step involves a monooxygenation of one of the terminal nitrogen atoms of the guanidine functionality of arginine with the formation of N^G-hydroxy-L-arginine (NOHA). This is followed by further oxidation and oxygenation of the oxime and guanidino groups of NOHA, resulting in the cleavage

* To whom correspondence should be addressed. M.S.: phone, (803) 576-5773; fax, (803) 777-9521; e-mail, sono@mail.chem.sc.edu. J.H.D.: phone, (803) 777-7234; fax, (803) 777-9521; e-mail, dawson@sc.edu.
[‡] University of South Carolina.
[§] Cleveland Clinic Foundation.
[||] The Scripps Research Institute.
[⊥] Tohoku University.
[#] Case Western Reserve University.
[▽] School of Medicine, University of South Carolina.

[1] Abbreviations: NO, nitric oxide; NOS, nitric oxide synthase; nNOS, eNOS, and iNOS, neuronal, endothelial, and inducible (macrophage) nitric oxide synthases, respectively; nNOS (HD), the oxygenase (heme) domain of neuronal nitric oxide synthase; P450, cytochrome P450; P450-CAM, cytochrome P450 from *Pseudomonas putida*; Mb, myoglobin; CCP, cytochrome *c* peroxidase; sGC, soluble guanylate (or guanylyl) cyclase; NOHA, N^G-hydroxy-L-arginine; BH₄, (6*R*)-5,6,7,8-tetrahydrobiopterin; DTT, dithiothreitol; UV−vis, UV−visible; MCD, magnetic circular dichroism; EPR, electron paramagnetic resonance; EPPS, *N*-(2-hydroxyethyl)piperazine-*N*′-3-propanesulfonic acid; MES, 2-(*N*-morpholino)ethanesulfonic acid; HEPES, *N*-(2-hydroxyethyl)-piperazine-*N*′-2-ethanesulfonic acid; DMSO, dimethyl sulfoxide; DMF, *N*,*N*-dimethylformamide; DMS, dimethyl sulfide; THF, tetrahydrofuran.

of the initial oxime C=N bond with the formation of L-citrulline and NO (*9*).

Among the three isoforms, nNOS and eNOS are constitutively expressed while iNOS is an inducible enzyme. All three NOS's contain two domains: an N-terminal oxygenase domain [or heme domain (HD)] and a C-terminal reductase domain. The oxygenase domain binds two prosthetic groups, heme (iron protoporphyrin IX) and (6*R*)-tetrahydrobiopterin (BH$_4$), and the substrate L-Arg or NOHA. The reductase domain contains tightly bound FMN and FAD and a binding site for NADPH. For NOS to be catalytically active, it must be a homodimer that is formed by an interaction of two oxygenase domains. For nNOS and eNOS, binding of a Ca^{2+}−calmodulin complex to a site located in the middle of the two domains then initiates NO synthesis by triggering heme reduction with the reductase domain, while iNOS contains tightly bound Ca^{2+}−calmodulin, and thus its catalytic activity is independent of a medium Ca^{2+} concentration.

NOS has been identified to be closely related to cytochrome P450 (P450) in terms of spectroscopic and catalytic properties although these two enzymes belong to different gene families (*10*). Like P450, the heme iron of NOS is cysteine thiolate-ligated (*11−13*), and the NOS reaction involves oxygen transfer, i.e., monooxygenation of organic substrates. The heme environments in NOS and P450, however, differ significantly. While the active site of P450 and its substrates are predominantly hydrophobic, several polar or ionic residues exist around the substrate-binding site of NOS including the bound substrate L-Arg itself. Further, the two conserved aromatic amino acid residues Phe-584 and Trp-409 engage in aromatic stacking with the NOS heme on its distal and proximal sides, respectively (*14*). The crystal structures of eNOS and iNOS heme domains reveal that the indole nitrogen of Trp-409 in nNOS forms a hydrogen bond with the heme-ligated cysteine thiolate (*11−14*).

A considerable fraction of the nNOS heme binds self-generated NO and remains as a ferrous−NO form during a steady state of NO synthesis (*15*). The ferrous heme−NO complex (*16*) thus formed is catalytically inactive but upon its interaction with O$_2$ reverts back to the active, ferric enzyme. Recently, it was found that mutation of the Trp-409 residue to Tyr or Phe in nNOS causes an increase in apparent maximum NO synthesis rate in comparison with the wild-type enzyme (*14*). This was later attributed to the fact that these two W409 mutants have less heme−NO complex buildup during the catalysis due to a faster decay of their ferrous−NO complexes under O$_2$ (*17, 18*). Further, resonance Raman studies of the Trp-409 mutants have shown that their ferrous−NO complexes are predominantly five coordinate (*19*).

To further understand the observed effects of the W409Y and W409F mutations on the nNOS catalysis on the active site structure level, we have employed UV−vis absorption, magnetic circular dichroism (MCD), and EPR spectroscopy in this study. MCD spectroscopy has been shown to be a powerful fingerprinting tool that allows one to determine the oxidation, ligation, and spin states of the metal center and to identify heme iron axial ligands (*20, 21*). EPR spectroscopy is useful in characterizing the electronic and thus the coordination structure of ferrous−NO heme complexes, which are paramagnetic species. Using these techniques, we

have observed a noticeable destabilization of the Fe−S bond in the ferrous−NO state caused by these mutations to Trp-409.[2]

EXPERIMENTAL PROCEDURES

Materials. CO and NO gases were obtained from Matheson Co. BH$_4$ was purchased from Biochemicals International. All other chemicals were purchased from Sigma or Aldrich and used as received. NO gas was passed through a NaOH (solid) column (2.5 cm × 20 cm) to remove contaminating oxidation products of NO.

Wild-Type and Mutant Heme Proteins. The heme domains (HD) of wild-type nNOS and its W409Y and W409F mutants were expressed in *Escherichia coli* and purified as described previously (*14, 22*). Construction, expression, and purification of H93G human Mb (*23, 24*), H93Y human Mb (*25*), and H175G CCP (*26*) were carried out as published. The β1(1−385) subunit of sGC was expressed in *E. coli* and purified also as reported (*27*).

Preparations of Samples for UV−Vis Absorption and MCD Spectroscopy. A solution (∼300 μL) of purified ferric NOS W409Y or W409F or wild-type nNOS (HD) (∼50 μM) was placed into a 0.2 cm anaerobic cuvette with a rubber septum-sealed joint with 40 mM EPPS, pH 7.5, containing 10% (v/v) glycerol, 1 mM DTT, 4 μM BH$_4$, 1 mM L-Arg, and 130 mM NaCl. After the ferric state was examined, the cuvette was extensively purged on ice over 30 min with a continuous flow of nitrogen through two syringe needles into and out of the headspace of the sample cuvette with occasional gentle shaking. NO gas was then introduced to the headspace and mixed into the sample solution by gentle shaking. Formation of the ferric−NO state was monitored by the overall spectral change. The ferric−NO species was then reduced with a few grains of solid sodium dithionite that was added to the sample through the opening of a wide gauge needle hole to give the ferrous−NO species. For another set of experiments, the oxygenase domains were examined in a sequence of ferric, ferrous−deoxy, and ferrous−CO forms as described previously for native full-length nNOS (*28*).

Ferrous−NO H175G CCP (50−60 μM) was prepared in 100 mM MES buffer, pH 6.0, by dithionite reduction of the ferric−NO protein as described above for the nNOS (HD). The ferrous−NO forms of H93G Mb (cavity mutant) and H93Y Mb were prepared as described elsewhere (*29*). For the ferrous−NO sGC experiments, a solution (∼300 μL) of ferrous−deoxy sGC [which is stable even under aerobic conditions (*30*)] was placed into a 0.2 cm anaerobic cuvette with 50 mM HEPES buffer, pH 7.4, containing 200 mM NaCl. The sample cuvette was extensively purged with nitrogen gas, and then NO gas was introduced to the headspace to generate ferrous−NO complex. Addition of sodium dithionite did not cause any further spectral change.

Ferrous−NO heme complexes were prepared in a cuvette under anaerobic conditions in tetrahydrofuran (THF), dimethyl sulfoxide (DMSO), *N,N*-dimethylformamide (DMF), and dimethyl sulfide (DMS) that had been thoroughly purged

---

[2] A major part of this work was presented in September 2001 at the Southeastern Regional Meeting of the American Chemical Society in Savannah, GA.

Table 1: Electronic Absorption (UV−Vis) Spectral Features of the Heme Domain (HD) and Full-Length nNOS Derivatives

derivative		absorption, λ_{max}, nm (ϵ, mM cm^{-1})		
		Soret	visible	
wild-type nNOS (HD)	ferric	393.5 (85.2)	505.5 (15.1)	646.5 (5.6)
	ferrous−deoxy	412.0 (72.3)	552.5 (12.8)	
	ferric−NO	439.5 (65.0)	546.0 (12.7)	576.5 (9.4)
	ferrous−CO	443.0 (106.1)	552.5 (11.4)	
	ferrous−NO	436.0 (67.0)	567.5 (11.8)	
W409Y nNOS (HD)	ferric	395.0 (85.1)	502.0 (12.2)	640.5 (5.4)
	ferrous−deoxy	409.0 (72.5)	550.0 (12.2)	
	ferric−NO	437.0 (65.0)	544.5 (13.2)	575.0 (10.2)
	ferrous−CO	445.5 (88.7)	542.0 (12.2)	
	ferrous−NO	406.5 (72.0)	559.0 (10.8)	
W409F nNOS (HD)	ferric	393.5 (85.9)		640.0 (5.9)
	ferrous−deoxy	411.0 (78.0)	552.0 (13.8)	
	ferric−NO	436.5 (64.5)	544.0 (13.1)	574.5 (10.2)
	ferrous−CO	446.5 (71.2)	531.5 (13.4)	
	ferrous−NO^a	406.5 (59.6)	559.5 (11.6)	
wild-type full-length nNOS^b	ferric	393.5 (100)		642.0 (7.3)
	ferrous−deoxy	411.5 (79.5)	554 (13.5)	
	ferric−NO	441 (93.3)	557 (14.2)	574 (11.1)
	ferrous−CO	446 (120)	551.5 (12.6)	
	ferrous−NO	436.5 (78.7)	564.5 (12.6)	

^{a} Has a shoulder at ∼436 nm. ^{b} From ref *28* except for ferric−NO species.

with nitrogen for about 1 h at room temperature (DMSO, DMF) or on ice (THF, DMS). Microliter volumes of hemin chloride stock solution (∼10 mM in DMSO) were diluted in ∼500 μL of the anaerobic solvents. The samples were further purged for ∼10 min after addition of heme. When NO gas was gently bubbled into the samples, the ferric− NO heme complex was formed slowly in DMSO (∼50% formed in 30 min at 25 °C). In THF, DMF, and DMS, the ferrous−NO complexes were prepared by first reducing the heme with sodium dithionite and then adding NO gas into the ferrous heme solutions. Three microliters of a sodium dithionite solution (20 mg/mL deionized water) was added to produce the ferrous−NO species in DMSO.

Preparation of EPR Samples. The ferrous−NO complex of W409Y NOS (∼90 μM) was prepared by reduction with a 5-fold excess of a sodium dithionite solution, followed by the addition of a small aliquot of a saturated NO solution (prepared by bubbling NO through an oxygen free solution) before being loaded into a 4 mm quartz EPR tube and frozen in liquid nitrogen. The sample was kept strictly anaerobic throughout by use of a glovebox with a N$_2$ atmosphere.

Low-Temperature Experiments. The ferrous−NO complex was prepared in a mixed solvent [40% (v/v) EPPS buffer (as described above) and 60% ethylene glycol] by adding NO gas into a thoroughly evacuated cuvette containing the dithionite-reduced (at 4 °C) mutant while keeping the cuvette in a dry ice/butanol bath (−54 °C). A spectral change was examined at −40 °C.

UV−Vis Absorption, MCD/CD, and EPR Spectroscopy. UV−vis absorption spectra were recorded on a Varian/Cary 210 or 219 spectrophotometer interfaced to an IBM PC using customized spectral acquisition software. MCD/CD spectra were recorded on a Jasco J500-A (at an initial stage) as described elsewhere (*31*) or a Jasco J600 spectropolarimeter equipped with a Jasco MCD-1B electromagnet operated at a magnetic field of 1.41 T. The J-600 was interfaced to an IBM-compatible computer via an RS-232C interface box by using software designed for Microsoft Window especially for the J-600 spectropolarimeter by the Jasco Corp. Noise

reduction was accomplished using the J600 FFT (fast Fourier transform) software and normalization to concentration, path length, and magnetic field strength (tesla) followed (M^{-1} cm^{-1} T^{-1}) (*31*, *32*). Sample integrity was checked by recording the absorption spectra of samples before and after each MCD/CD measurement with less than 5% spectral changes deemed acceptable. All spectra were taken at 4 °C unless otherwise noted using 0.1, 0.2, or 1 cm anaerobic quartz cuvettes.

EPR spectra were recorded on a Bruker ESP X-band spectrometer using a TE102 rectangular cavity maintained at low temperature by an Air Products LTR-3 liquid helium cryostat; sample temperature was measured with a calibrated GaAs diode.

RESULTS

Extinction Coefficients (ϵ Values) for Wild-Type and W409 Mutant nNOS (HD). Since the extinction coefficients reported from different laboratories for the same isoforms of NOS vary to a significant extent (*33*), we determined the ϵ values for the wild-type nNOS (HD) and its mutants, W409Y and W409F, using the pyridine hemochromogen method (*28*). The ϵ values thus determined for the Soret band for the BH$_4$-containing L-Arg-bound high-spin ferric nNOS (HD) (ϵ_{393} = 86 ± 2 mM^{-1} cm^{-1}) were found to be essentially identical for the three proteins.

UV−Vis Absorption and MCD Spectra of High-Spin Ferric, Ferric−NO, Ferrous−Deoxy, Ferrous−CO, and Ferrous−NO States of nNOS (HD). In this study, the heme domains of wild-type nNOS and of the W409Y and W409F nNOS mutants have been examined with both BH$_4$ and L-Arg bound. Selected UV−vis spectral parameters for all three nNOS (HD) proteins together with those for full-length nNOS in their ferric and ferrous oxidation states in five ligation forms are summarized in Table 1 (MCD spectral parameters are in the Supporting Information, Table S1). The UV−vis absorption and MCD spectra of the high-spin ferric W409Y, W409F, and wild-type nNOS (HD) are plotted
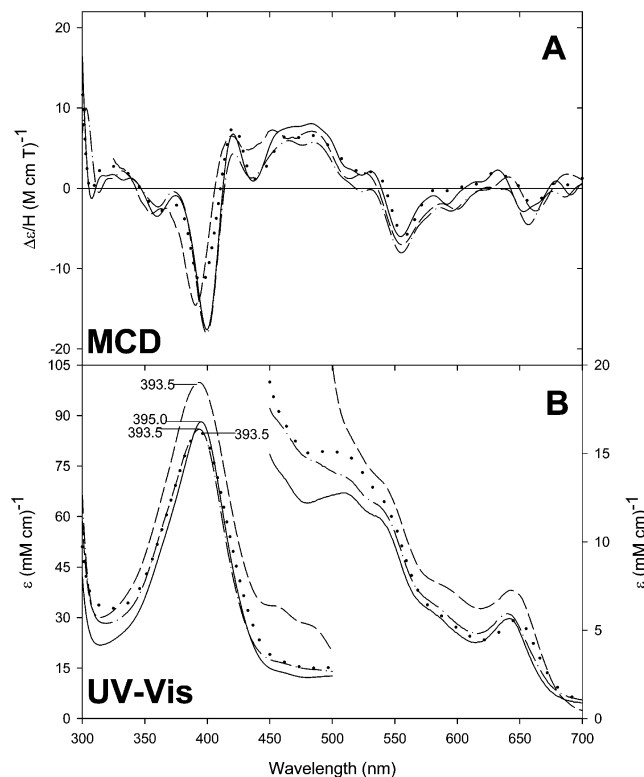
FIGURE 1: MCD (A) and UV−vis absorption (B) spectra of ferric wild-type nNOS (HD) (dotted line) plotted together with those of ferric W409Y (HD) (solid line) and W409F (HD) (dash−dotted line) and of full-length nNOS (short-dashed line). Heme domain (HD) concentrations were ∼50 μM. The data of the full-length nNOS were taken from ref. *28*.

FIGURE 2: MCD (A) and UV−vis absorption (B) spectra of wild-type ferric−NO nNOS (HD) (dashed line) plotted together with those of ferric−NO W409Y (HD) (solid line) and W409F (HD) (dotted line).

together in Figure 1 with the corresponding spectra of full-length nNOS reported previously (*28*). All four proteins exhibit very similar UV−vis absorption and MCD spectra except for minor differences in the UV−vis absorption charge-transfer band (high-spin marker) position (646.5 nm for the wild-type protein vs ∼640 nm for the two mutants) and in the Soret MCD trough intensity. As pointed out elsewhere (*34*), the absorption spectral intensity for full-length nNOS ($\epsilon_{Soret} = \sim100$ mM^{-1} cm^{-1}) is noticeably greater in the 300−700 nm region than those for the oxygenase domains due to the presence of the flavin and flavin semiquinone groups for the former. On the other hand, the MCD spectra for the three oxygenase domains are not significantly different from those of the wild-type full-length nNOS (except for some minor differences in intensity, line shape, and trough position in the 350−450 nm region) because of the negligible MCD signals of the flavins (*34*).

The UV−vis absorption and MCD spectra of ferric−NO W409Y, W409F, and wild-type nNOS (HD) are plotted together in Figure 2. Ferric−NO NOS has not previously been characterized with MCD spectroscopy. In the UV−vis absorption spectra, there are two sharp peaks in the visible region (500−700 nm) at 544 and 575 nm; in the Soret region (300−500 nm), a prominent peak at ∼437 (mutants) or ∼440 nm (wild type) and an additional band at ∼370 nm are seen. The MCD spectra consist of three derivative-shaped features centered about 445, 540, and 580 nm.

The UV−vis absorption and MCD spectra for the ferrous−deoxy and ferrous−CO states for the wild-type nNOS (HD) and the two mutants of the nNOS (HD) (spectra not shown
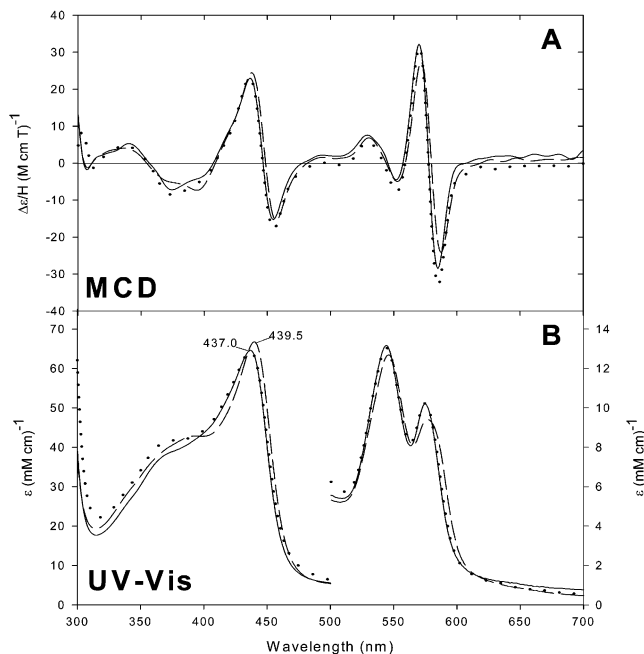
here but included as Supporting Information, Figures S1 and S2) are quite similar to the corresponding spectra of the full-length nNOS (*28*). Both mutants and the wild-type oxygenase domain exhibit Soret absorption peaks at 409−412 nm in the ferrous−deoxy state[3] and at 443−446.5 nm in the ferrous−CO state.

Optical Absorption and MCD Spectra of the Ferrous−NO Complex of the nNOS (HD). In Figure 3, the UV−vis absorption and MCD spectra of the ferrous−NO adducts of the W409Y, W409F, and wild-type nNOS (HD) are overlaid. Unlike the other states described above, the ferrous−NO derivatives of the two mutants[4] exhibit Soret absorption peaks that are markedly blue shifted with respect to that of the wild-type species (Soret peak at 406.5 nm vs 436 nm, Figure 3B). In addition, new UV−vis absorption bands at ∼480 nm appear for the two mutants although the band for the W490F mutant is not so obvious. These spectral features, especially the occurrence of the ∼480 nm absorption band, are characteristic of known five-coordinate ferrous−NO heme complexes (*36*) (vide infra). The MCD spectra of the

---

[3] A relatively small but reproducible absorption band is observed at ∼640 nm only for the W409Y nNOS (HD) mutant in its dithionite-reduced ferrous−deoxy state (Figure S1). Considering that dithionite has a very low midpoint potential (E_m) ($E_m \leq -470$ mV at $\leq10^{-3}$ M dithionite at pH 7.0 and 25 °C, estimated by E_m (mV) = $-386 + 29$ log [dithionite]) (*35*), it is unlikely that the absorption band is due to the incompletely reduced ferric heme domain.

[4] The ferrous−NO species of both W409Y and W409F nNOS (HD) mutants were somewhat unstable. Shortly (10−15 min) after initial formation of the ferrous−NO species at 4 °C, the mutant protein solutions slowly started to become turbid. This denaturation was slow enough not to significantly interfere with the UV−vis absorption and MCD spectral measurements even 30 min after preparation except for slight absorption increases. Even at low temperatures (−40 °C) in a cryogenic solvent (60% ethylene glycol−40% aqueous buffer mixture, v/v), the slow denaturation could not be prevented. No detectable denaturation was observed for the ferrous−NO wild-type nNOS (HD) under the same conditions or for the other forms of the two mutants examined in this study.
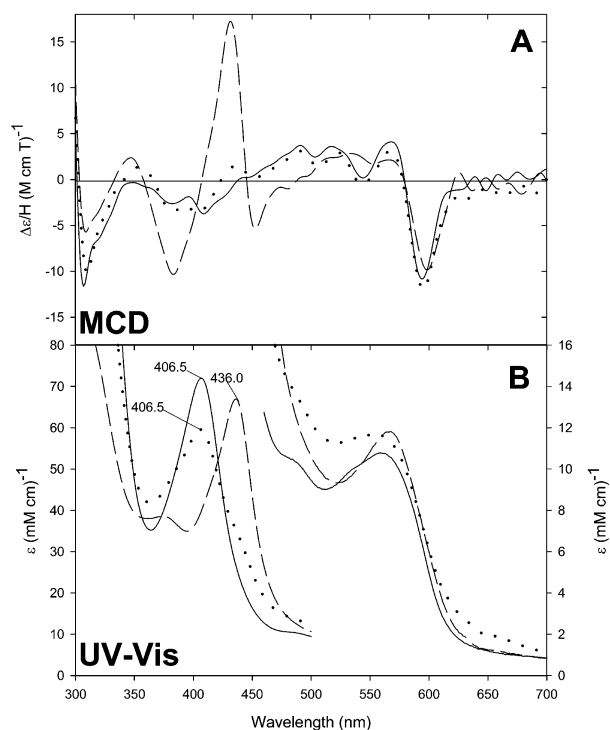
FIGURE 3: MCD (A) and UV−visible absorption (B) spectra of wild-type ferrous−NO nNOS (HD) (dashed line) plotted together with those of ferrous−NO W409Y nNOS (HD) (solid line) and W409F nNOS (HD) (dotted line). The large absorbance below 360 nm in (B) was due to the presence of excess amounts of dithionite (λ_{max} = 315 nm). This dithionite absorbance smaller than 2 does not significantly affect the MCD spectra of these nNOS heme domains in the wavelength region.
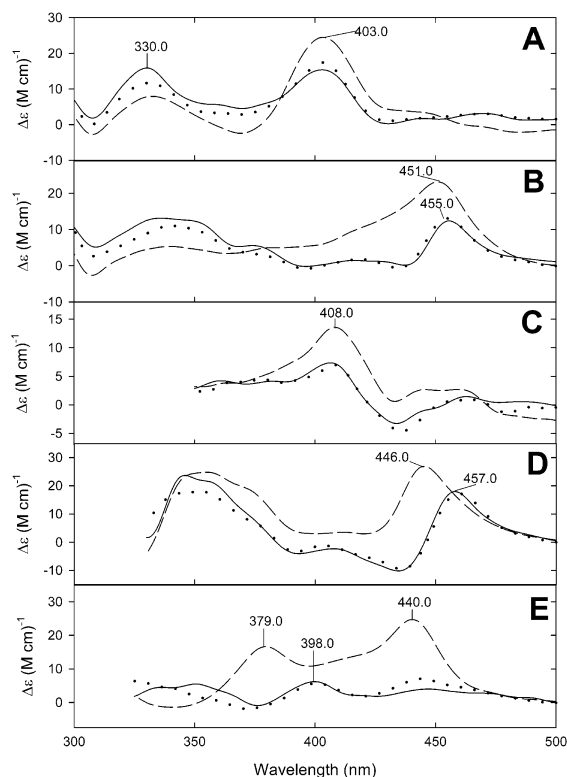

FIGURE 4: CD spectra of various states of the heme domains of W409Y (solid line), W409F (dotted line), and wild-type nNOS (dashed line): (A) ferric, (B) ferric−NO, (C) ferrous−deoxy, (D) ferrous−CO, and (E) ferrous−NO states.

mutants (Figure 3A and Table S1) are also noticeably different from that of the wild-type protein in the Soret region. The MCD spectrum of the latter is typical of a six-coordinate thiolate-ligated ferrous−NO species (*28*) exhibiting an inverted V-shaped predominant peak (~430 nm) and two less intense troughs (~380 and ~450 nm) in the Soret region. These Soret MCD spectral patterns are completely lost in the spectra of the two mutants, which have considerably less intense and rather featureless band patterns below 450 nm; two weak troughs ($|\Delta\epsilon/H| \approx 3.5$ M⁻¹ cm⁻¹ T⁻¹) at ~380 and ~405 nm are seen. The visible region MCD spectra of the ferrous−NO adducts of the two mutants and of the wild-type (HD) protein are more or less similar to each other with peaks at 520−525 and ~570 nm and a prominent trough at 595−600 nm.

The UV−vis and MCD spectra of ferrous−NO W409Y and W409F NOS are generally similar to each other, but some minor differences are clearly seen as evident in their Soret region UV−vis absorption spectra (Figure 3B, solid vs dotted lines). Upon dithionite reduction of the ferric−NO W409Y nNOS (HD) at 4 °C, the ferrous−NO species (406.5 nm) was formed without detectable intermediates (e.g., a 436 nm species). Furthermore, no spectral evidence of a six-coordinate ferrous−NO species (436 nm) was detected for the W409Y mutant even at −40 °C.

On the other hand, for the W409F mutant, an absorption peak at ~436 nm was initially observed, which gradually decreased in parallel with an increase in the 406.5 nm peak. The spectral conversion was complete in ~30 min at 4 °C accompanying a single set of isosbestic points at ~427 and

~465 nm. However, the initial 436 nm peak for the W409F nNOS (HD) mutant did not disappear completely (Figure 3B, dotted line) even after additional prolonged incubation at 4 °C. Similar results have been reported for the full-length counterparts of the two mutants although the final absorption peaks (~417 nm) appear to be considerably more red shifted for the full-length proteins (*17*). On the basis of both UV−vis and MCD spectral simulation (not shown) and estimation, the present results indicate that both ferrous−NO W409F and W409Y NOS(HD) are a mixture of the 406.5 nm (presumably five-coordinate) form (~85% and ~95%, respectively) and the minor 436 nm (six-coordinate) form (~15% and ~5%, respectively).

Circular Dichroism (CD) Spectra of nNOS (HD) Derivatives. In Figure 4, CD data in the Soret region (300−500 nm) are plotted together for the oxygenase domain of wild-type, W409Y, and W409F nNOS for the various oxidation and ligation states as described in the earlier section. For each species, the W409Y and W409F mutants are similar to each other, but they clearly differ from the wild-type nNOS even though the UV−vis absorption spectra are quite similar for the analogous states for the three nNOS (HD) (Figures 1, 2, S1, and S2 and Table 1) except in regard to the ferrous−NO species (Figure 3). The CD differences in the Soret region between the wild type and the W409 mutants most likely reflect the change from heme−tryptophan (aromatic amino acid) $\pi-\pi$ electronic interaction to heme−tyrosine or −phenylalanine $\pi-\pi$ electronic interactions as interpreted for the origin of the CD signal for Mb (*37*). The CD spectral similarities for the W409Y and W409F nNOS (HD) suggest that the heme environmental structures for the two mutants are not significantly different, despite the presence of a
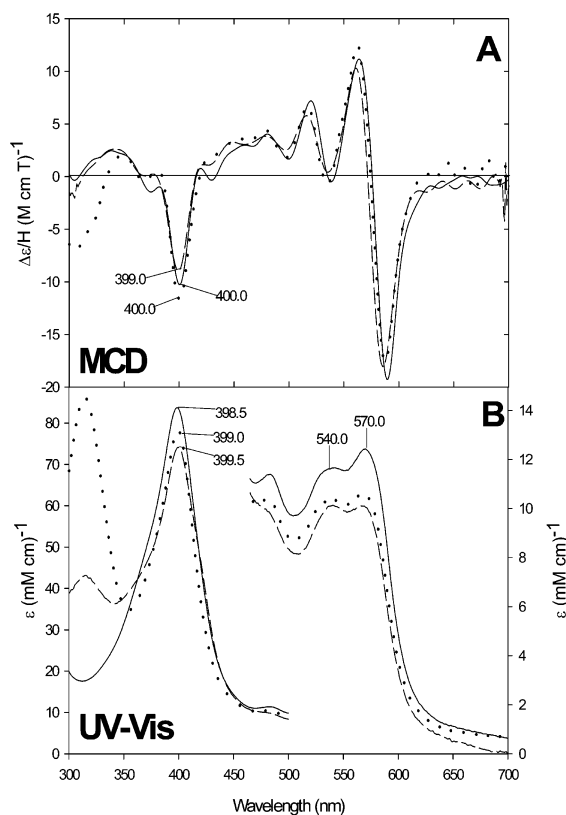
FIGURE 5: MCD (A) and UV−vis absorption (B) spectra of ferrous−NO species: soluble guanylate cyclase (sGC) (solid line), H93G Mb with 0.1 mM imidazole (dashed line), and H93Y Mb (dotted line), all at ∼50 μM. The MCD spectrum of the H93G Mb was from ref *29*.

FIGURE 6: MCD (A) and UV−vis absorption (B) spectra of the ferrous−NO complex of the cavity H93G without imidazole (dashed line) and cavity H175G CCP with imidazole (18 mM) (solid line). Sample concentrations were ∼50 μM. Ferrous−NO H93G Mb was prepared by stepwise microliter additions of dithionite solution to an anaerobic ferric−NO H93G solution until it was completely reduced. See the legend to Figure 3 for the absorbance interference by the excess dithionite below 360 nm for the CCP spectrum.

hydroxyl group, a potential hydrogen bond donor, at the 409 residue position for the former mutant. Although we did not make any attempt to further interpret the CD data, it is unlikely that the CD differences are the result of large protein structural change(s) around the heme upon W409Y or W409F mutation because these mutants are catalytically active (*14, 17*).

Optical Absorption and MCD Spectral Properties of Three Representative Five-Coordinate Ferrous−NO Heme Proteins. Figure 5 shows the UV−vis absorption and MCD spectra for three five-coordinate ferrous−NO heme protein adducts: soluble guanylyl cyclase (sGC), H93G Mb in the presence of low imidazole concentration (0.1 mM), and H93Y Mb. These are all known five-coordinate ferrous− NO species that have previously been characterized with resonance Raman (*38−41*), EPR (except for H93Y Mb) (*39, 41, 42*), and, for H93G Mb only, MCD (*29*) spectroscopy. The spectra of all three of these ferrous−NO species are similar in overall pattern with a Soret absorption peak at around 400 nm as well as two relatively broad peaks in the visible region around 540 and 570 nm along with the characteristic peak at 480 nm described above. In the MCD spectra, there is a prominent trough around 400 nm with an intensity of about −10 M^{-1} cm^{-1} T^{-1}.

Optical Absorption and MCD Spectral Properties of Additional Five-Coordinate Ferrous−NO Heme Proteins. Figure 6 shows the UV−vis absorption and MCD spectra of the ferrous−NO adduct of H93G Mb in the absence of imidazole and that of H175G CCP in the presence of a low
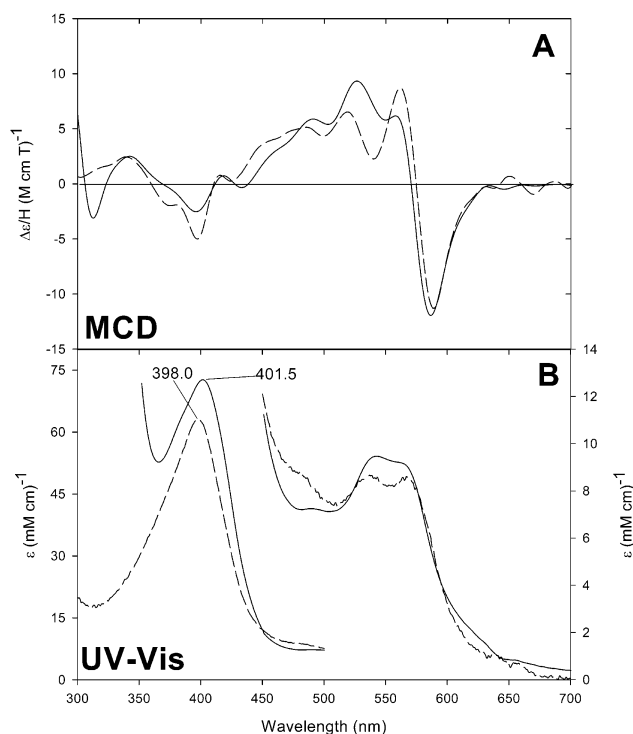
concentration of imidazole. The cavity mutant of Mb forms a predominantly five-coordinate ferrous−NO complex even in the presence of a relatively low concentration (<1 mM) of imidazole as judged by EPR, resonance Raman, and MCD spectroscopy (*29, 39*). The EPR spectrum of the ferrous− NO complex of this CCP mutant exhibited a pattern typical of a five-coordinate adduct (i.e., a sharp triplet splitting at *g* = ∼2.01) both in the absence and in the presence of added exogenous imidazole (*43*). The MCD spectra of the ferrous− NO derivatives of these two cavity mutants exhibit less intense troughs at ∼400 nm (five coordinate) as well as an additional peak/trough combination feature centered around 425 nm.

Optical Absorption and MCD Spectral Properties of Five-Coordinate Ferrous−NO Heme Complexes in Organic Solvents. Figure 7 shows the UV−vis absorption and MCD spectra of the ferrous−NO heme model adducts in THF, DMSO, DMF, and DMS. The complexes in these organic solvents have been previously examined with UV−vis absorption (*36, 44, 45*), EPR (*45*), and IR (*36, 45*) spectroscopy. These organic solvents contain oxygen (THF, DMSO, DMF) and sulfur (DMS) atoms as potential donor ligands that could coordinate to the heme iron of the ferrous−NO species. However, the ferrous−NO heme species in all four solvents has been shown to be a largely five-coordinate species at ambient temperatures using these spectroscopic techniques (*36, 44, 45*). This is borne out with the present data in that the ferrous−NO heme adducts in all four solvents exhibit UV−vis absorption peaks around 400 nm and a noticeable band near 480 nm, as expected for five-coordinate
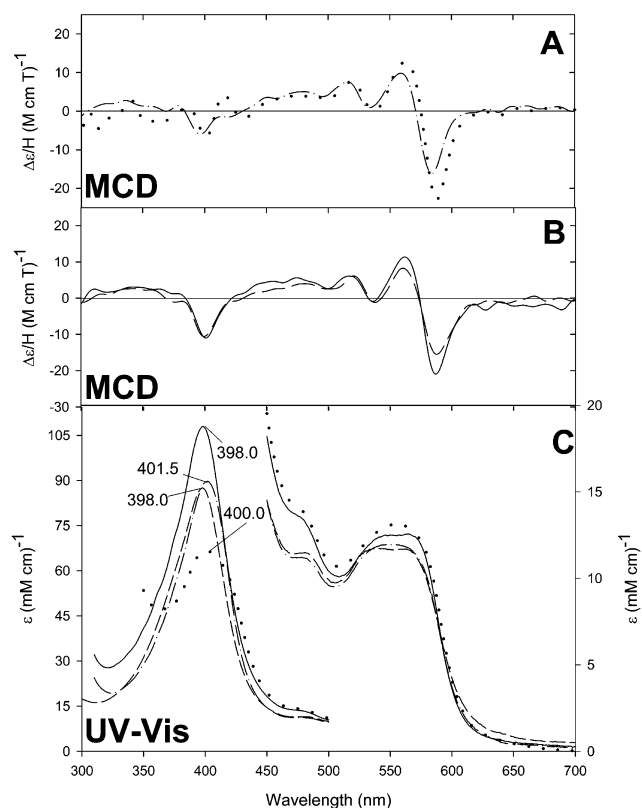
FIGURE 7: MCD (A and B) and UV−vis absorption (C) spectra of the ferrous−NO heme in THF (solid line), DMSO (dash−dotted line), DMF (dashed line), and DMS (dotted line). Sample (heme) concentrations were ~50 µM.
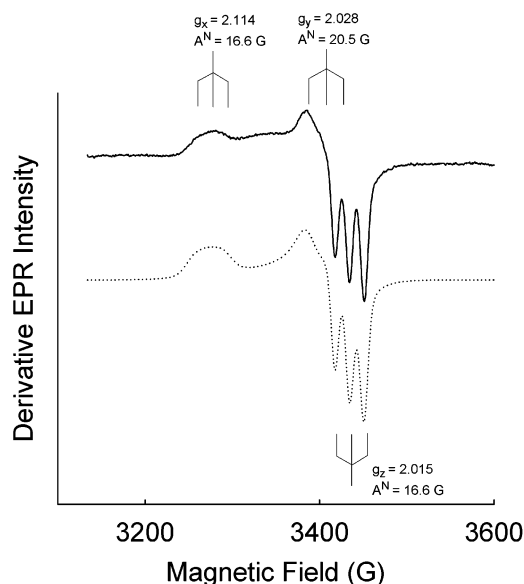

FIGURE 8: EPR spectrum of the ferrous−NO adduct of W409Y nNOS (HD) (solid line) together with the simulated spectrum (dotted line). The EPR signal of the sample (~90 µM) was measured at 4.0 K at a frequency of 9.68 GHz and 0.4 mW. The modulation amplitude was 10 G at a modulation frequency of 100 kHz. For the simulation (dotted line), *g* values of 2.114, 2.0275, and 2.015 and corresponding hyperfine constants of 16.6, 20.5, and 16.6 G were used.

species (*36*, *46*). In addition, the Soret region MCD spectra feature the same weak trough near 400 nm that is characteristic of five-coordinate ferrous−NO adducts. In the visible region (500−700 nm), the MCD spectral line shapes and band intensities are generally similar to each other in all four solvents. A peak/trough feature around 425 nm is also detectable in the MCD spectra in DMSO and especially in DMS.

EPR Spectrum of the Ferrous−NO State of W409Y nNOS (HD). The EPR spectrum of the ferrous−NO complex of W409Y nNOS (HD) is shown in Figure 8 (solid line) together with the simulated spectrum (dotted line). The component of the spectrum at *g* = ~2.01 shows three hyperfine transitions consistent with coupling of the $S = \frac{1}{2}$ spin to a single ^{14}N nucleus. While this would be expected for the nitrosyl complexes of both six-coordinate thiolate-ligated and five-coordinate forms, several details of the spectrum are distinct from those of wild-type NOS (*47*). First, the hyperfine coupling (A^N) of 16.6 G seen in the mutant is smaller than that ($A^N = 20−22$ G) seen in wild-type NOS (*47*, *48*). Instead, it is more typical of A^N values of 16−17 G that have been observed in five-coordinate nitrosyl complexes of H93G Mb (*39*), sGC (*42*), H175G CCP (*43*), and the P420 forms of pterin-free nNOS (*48*) as well as of several P450s (*49*, *50*). Second, the overall line shape of the signal in Figure 8 is characteristic of the P420 forms (five coordinate) of NOS and P450s rather than the six-coordinate form. For the six-coordinate forms of these heme proteins, a signal with rhombic *g* values at ~2.08, ~2.005, and ~1.97 is observed (*47*, *49*, *50*). In contrast, the spectrum in Figure 8 can be simulated (dotted line) with nearly axial *g* values

of 2.114, 2.0275, and 2.015 and corresponding hyperfine constants of 16.6, 20.5, and 16.6 G, respectively. Thus, the EPR spectrum shown in Figure 8 argues against the presence of thiolate ligation in the ferrous−NO nNOS (HD) mutant.

DISCUSSION

Tryptophan-409 plays important roles in regulating the activity of nNOS. Mutations of Trp-409 to Phe and Tyr lead to significant increases in NO synthesis activity (by 1.5−3 times) compared to the wild-type enzyme (*14*). In contrast to the wild-type enzyme, little or none of the ferrous−NO form of the enzyme (exhibiting a Soret peak at ~436 nm) builds up during enzymatic NO synthesis with either the W409F or W409Y mutant. This is possibly due to the diminished stability of that complex in the mutants under aerobic conditions compared to the wild-type enzyme (*17*, *18*), although the exact mechanism of this phenomenon is unclear at present. On the other hand, the W409H nNOS mutant was reported to have 4-fold lower NO synthase activity (*51*).

In a recent resonance Raman and UV−vis spectroscopic study, Rousseau, Stuehr, and co-workers (*19*) have demonstrated that the same two W409 nNOS (HD) mutants likely lose the cysteinate proximal ligand upon formation of the ferrous−NO complexes. However, while the observed porphyrin skeletal Raman bands for the ferrous−NO mutants were indicative of five coordination, the $\nu_{Fe−NO}$ Raman stretch, which was clearly seen for the six-coordinate wild-type Fe−NO state, was absent for the ferrous−NO complexes of the two mutants (*19*). This precluded a definitive conclusion that the ferrous−NO states of the two mutants are indeed five coordinate. For this reason, we have used MCD and EPR together with UV−vis spectroscopy in the present study to further characterize and to better understand

the unusual properties of the W409F and W409Y nNOS mutants, with particular emphasis on their ferrous−NO adducts. We have closely compared the spectral properties of the ferrous−NO complexes of the nNOS (HD) mutants with those of several other five-coordinate and six-coordinate ferrous−NO heme proteins or model systems.

The proximal cysteinate thiolate ligand has been proposed to play a key role in O−O bond cleavage during dioxygen activation by P450 (*52*) and, most likely, also by NOS. Heterolytic O−O bond cleavage leads to compound I (an oxo−ferryl porphyrin cation radical) as the reactive oxygen intermediate (*52*, *53*). Without the strong electron release of the thiolate, homolytic cleavage is favored and the less reactive oxo−ferryl compound II is formed (*54*). In all structurally characterized heme−thiolate proteins including P450-CAM and chloroperoxidase, hydrogen bonds between the thiolate sulfur and peptide NH groups are present to stabilize the heme iron-bound thiolate sulfur (*55*, *56*). NOS also has a cysteinate thiolate proximal ligand that has three hydrogen bonds (*7*, *11*) (see Figure 1 in ref 19 for structural presentations of the hydrogen bonds for the three proteins). One of the hydrogen bonds in nNOS involves the Trp-409 indole NH (*7*, *14*).

The influence that hydrogen bonding has on the properties of thiolate-ligated heme complexes has been previously examined through the synthesis of protein-free heme adducts with built-in hydrogen bond donors (*57*, *58*) or through site-directed mutagenesis of P450-CAM (*54*). The results have shown that the presence of NH···S hydrogen bonds to the thiolate sulfur shifts (raises) the redox potential of the heme iron (*54*, *57*, *58*), stabilizes the high-spin (five-coordinate) ferric state (*58*), or modifies the monooxygenase activity of the enzyme or model catalyst (*54*, *57*). Information about midpoint potential changes upon W409Y and W409F nNOS mutations is not available; however, it is known that removal of the L358 to proximal C357 hydrogen bond in P450-CAM results in a decrease of its midpoint potential by 36 mV (−134 to −170 mV) (*54*). The ferric H93C Mb mutant loses thiolate ligation upon reduction or upon formation of its ferrous−CO and ferrous−NO complexes (*25*), presumably due to the lack of hydrogen bond donation to stabilize the thiolate-ligated ferrous form of the protein. Thus, the major function of the Cys···HN hydrogen bonds appears to be to provide an electropositive environment for the negatively charged cysteinate (*56*, *58*) for stabilization of the thiolate−Fe bond and to regulate the heme redox potential (*58*). Furthermore, additional structural roles of the multiple hydrogen bonds in holding the sulfur donor atom in position for ligation should also be considered as in thiolate-ligated model complexes (*59*) where the thiolate ligand is tethered in place even without such hydrogen bonds.[5]

There are two types of ferrous−NO heme complexes: five and six coordinate. For six-coordinate cases, the ligands trans to NO can include cysteine thiolate, histidine imidazole, or, possibly, donor atoms from other amino acids, the peptide, or solvent. Ferrous−NO wild-type nNOS provides an example of a thiolate-ligated six-coordinate ferrous−NO species (Figure 9A). It has very characteristic UV−vis
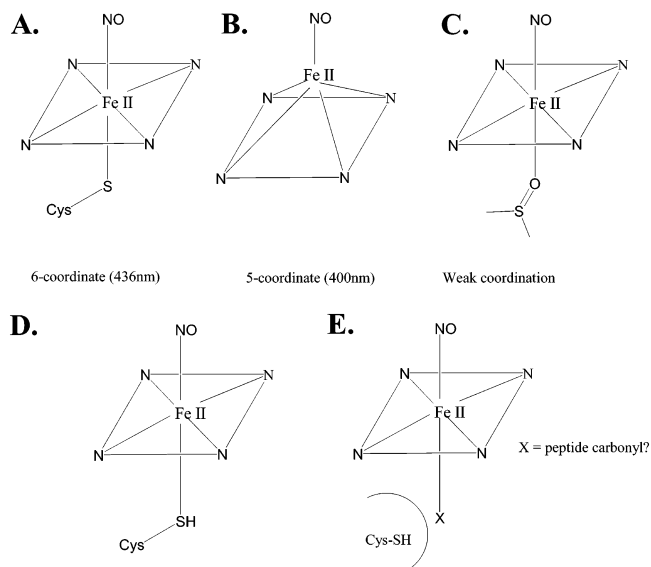

FIGURE 9: Coordination modes for ferrous−NO heme complexes. (A) A thiolate-ligated six-coordinate species. (B) A five-coordinate species. (C) A DMSO-ligated species. (D) A likely six-coordinate minor species produced from the W409Y and W409F mutants that has a cysteine thiol trans to NO. (E) An alternative possible species produced from the W409 mutations, which has lost cysteine thiolate ligation and has coordination of a peptide carbonyl group or another donor ligand (X).

absorption (Figure 3B, dashed line, Soret peak ∼436 nm) and MCD (Figure 3A, dashed line) spectral properties as described in the Results section. Histidine imidazole-ligated six-coordinate ferrous−NO species, as are found with heme proteins such as wild-type Mb, horseradish peroxidase, or CCP, exhibit a Soret absorption band at ∼420 nm and a derivative-shaped MCD spectral band pattern centered at ∼420 nm in the Soret region (*60*). Coordination by other donor ligands such as oxygen- (carboxylate, carbonyl, alcohol, or ether) or neutral sulfur- (thiol or thioether) containing ligands is also possible; UV−vis absorption and MCD spectral properties of such six-coordinate ferrous−NO complexes have not been reported.

Several examples of the UV−vis absorption and MCD spectra of five-coordinate ferrous−NO species are displayed in Figures 5−7. These complexes have unique spectral properties with a Soret absorption peak near 400 nm with an extra band at about 480 nm and a relatively weak but prominent single MCD trough at about 400 nm with intensity of −12 M^{-1} cm^{-1} T^{-1} or less. Close examination of the MCD spectra of the five-coordinate ferrous−NO heme protein complexes (Figures 5 and 6) and the ferrous−NO model complexes (Figure 7) reveals the presence of a minor peak/ trough combination centered near 425 nm for most of these complexes. Such a feature is more noticeable in the spectra of H93G Mb and H175G CCP (Figure 6A) and of the model complex in DMS (Figure 7A). This feature likely reflects the presence of a small amount of six-coordinate species.

The ferrous−NO derivatives of the two W409 mutants have almost entirely lost their cysteinate ligation (see Results) as indicated by their MCD spectra, which are dramatically different from that of the ferrous−NO wild-type protein (Figure 3) but generally similar to those of the various five-coordinate ferrous−NO complexes (Figures 5−7). However, the MCD spectra of the two nNOS mutants (Figure 3A)

---

[5] A thiolate-ligated ferrous−NO heme was successfully generated using a free heme in DMSO in the presence of a quite high concentration (0.3 M) of methanethiolate base with crown ether (*44*).

display some additional features not seen in the spectra of the five-coordinate ferrous—NO adducts. Rather than a single prominent trough at ~400 nm, either a single broad and weaker trough (W409F) or two weak troughs (W409Y) are seen. Examination of the overlaid spectra of the three ferrous—NO complexes (Figure 3A) suggests that the main difference seen between the spectra of the mutants and those of the other five-coordinate ferrous—NO complexes (Figures 5—7) is the presence of a small amount of thiolate-ligated six-coordinate complex or other type of six-coordinate species (see below). The MCD spectra of the two ferrous—NO mutants broadly resemble that of the ferrous—NO heme in DMSO (Figure 7A, dash—dotted line), which is also likely a mixture of five-coordinate (Figure 9B) (predominant species) and a minority six-coordinate species (Figure 9C) (*36, 46*). Thus, we conclude that the coordination modes of the ferrous—NO W409 nNOS (HD) mutants are likely a mixture of major five-coordinate (85—90%) and minor six-coordinate (10—15%) species.

A similar suggestion has also been made from a recent resonance Raman study of the ferrous—NO form of the same W409 (HD) mutants (*19*). The ligand trans to NO in the minor six-coordinate species could be a thiolate ligand (Figure 9A), as just discussed, or since the spectral properties of such species have yet to be characterized, it could be a protonated cysteine (RSH) (Figure 9D) or an oxygen donor atom such as from a peptide carbonyl (Figure 9E). The apparent absence of EPR signals from such a six-coordinate ferrous—NO species in the spectra of the W409Y nNOS (HD) (Figure 8) or in the H175G CCP (with and without imidazole) (*43*) is likely due to the difficulty in observing a 10—15% minority species whose spectrum directly overlaps that of the major complex.

The mutations of Trp-409 in nNOS have no major effect on the UV—vis absorption or MCD spectra of the ferric (Figure 1), ferrous—deoxy (Figure S1), ferric—NO (Figure 2), and ferrous—CO (Figure S2) derivatives. Only in the ferrous—NO state (Figure 3) are the UV—vis and MCD spectra (five-coordinate type) of the mutants dramatically different from those (six-coordinate type) of wild-type ferrous—NO nNOS. The significant difference between the ferrous—NO (predominantly five-coordinate) and the ferrous—CO (six-coordinate) complexes of the W409 nNOS (HD) mutants can be explained by the known opposite (repulsive vs cooperative, respectively) strong influences of NO and CO on the affinity of their trans ligands (*61*). Thus, the Fe—S bond, already weakened by removal of one of the three hydrogen bonds in the two W409 mutants (*19*), may be relatively easily broken upon formation of the ferrous—NO complex.

In summary, the ferrous—NO complexes of the W409Y and W409F nNOS (HD) mutants have clearly lost their cysteinate ligation and are almost entirely five coordinate. This conclusion is strongly supported by comparison of the MCD spectra of the ferrous—NO mutants with those of ferrous—NO complexes of known five- and six-coordinate heme proteins and models. The EPR spectrum of ferrous—NO W409Y nNOS (HD) further supports the same conclusion. Thus, the likely explanation for the differences in coordination in the ferrous—NO state and in the catalytic behavior of the W409Y/F nNOS mutants from those of wild-type nNOS is that the mutants lack one of the naturally occurring hydrogen bonds needed to fully stabilize the Fe—cysteinate sulfur bond.

SUPPORTING INFORMATION AVAILABLE

One table listing MCD parameters for the heme domain (HD) and full-length nNOS derivatives and two figures presenting MCD and UV—vis absorption spectra of the ferrous—deoxy (Figure S1) and ferrous—CO (Figure S2) derivatives of W409Y, W409F, and wild-type nNOS (HD). This material is available free of charge via the Internet at http://pubs.acs.org.

REFERENCES

1. Bredt, D. S., and Snyder, S. H. (1994) *Annu. Rev. Biochem. 63*, 175—195.
2. Ignarro, L. J. (1990) *Annu. Rev. Pharmacol. Toxicol. 30*, 535—560.
3. Hemmens, B., and Mayer, B. (1997) in *Methods in Molecular Biology* (Titheradge, M. A., Ed.) Vol. 100, pp 1—32, Humana Press, Totowa, NJ.
4. Griffith, O. W., and Stuehr, D. J. (1994) *Annu. Rev. Physiol. 57*, 707—736.
5. Stuehr, D. J. (1999) *Biochim. Biophys. Acta 1411*, 2146—2152.
6. Marletta, M. A., Hurshman, A. R., and Rusche, K. M. (1998) *Curr. Opin. Chem. Biol. 2*, 656—663.
7. Raman, C. S., Martásek, P., and Masters, B. S. S. (2000) in *The Porphyrin Handbook* (Kadish, K. M., Smith, K. M., and Guilard, R., Ed.) Vol. 4, pp 293—341, Academic Press, San Diego, CA.
8. Feldman, P. L., Griffith, O. W., and Stuehr, D. J. (1993) *Chem. Eng. News 71*(51), 26—38.
9. Jousserandot, A., Boucher, J., Henry, Y., Niklaus, B., Clement, B., and Mansuy, D. (1998) *Biochemistry 37*, 17179—17191.
10. Bredt, D. S., Hwang, P. M., Glatt, C. E., Lowenstein, C., Reed, R. R., and Snyder, S. H. (1991) *Nature 351*, 714—718.
11. Crane, B. R., Arvai, A. S., Ghosh, D. K., Wu, C., Getzoff, E. D, Stuehr, D. J., and Tainer, J. A. (1998) *Science 279*, 2121—2126.
12. Raman, C. S., Li, H., Martásek, P., Kral, V., Masters, B. S. S., and Poulos, T. L. (1998) *Cell 95*, 939—950.
13. Fishmann, T. O., Hruza, A., Niu, X. D., Fossetta, J. D., Lunn, C. A., Dolphin, E., Prongay, A. J., Reichert, P., Lundell, D. J., Narula, S. K., and Weber, P. C. (1999) *Nat. Struct. Biol. 6*, 233—242.
14. Adak, S., Crooks, C., Wang, Q., Crane, B. R., Tainer, J. A., Getzoff, E. D., and Stuehr, D. J. (1999) *J. Biol. Chem. 274*, 26907—26911.
15. Abu-Soud, H. M., Wang, J., Rousseau, D. L., Fukuto, J. M., Ignarro, L. J., and Stuehr, D. J. (1995) *J. Biol. Chem. 270*, 22997—23006.
16. Noguchi, T., Sagami, I., Daff, S., and Shimizu, T. (2001) *Biochem. Biophys. Res. Commun. 282*, 1092—1097.
17. Adak, S., Wang, Q., and Stuehr, D. J. (2000) *J. Biol. Chem. 275*, 17434—17439.
18. Adak, S., and Steuhr, D. J. (2001) *J. Inorg. Biochem. 83*, 301—308.
19. Couture, M., Adak, S., Stuehr, D. J., and Rousseau, D. L. (2001) *J. Biol. Chem. 276*, 38280—38288.
20. Dawson, J. H., and Dooley, D. M. (1989) in *Iron Porphyrins* (Lever, A. B. P., and Gray, H. B., Eds.) Part 3, pp 1—135, VCH, New York.
21. Cheek, J., and Dawson, J. H. (2000) in *Handbook of Porphyrins and Related Macrocycles* (Kadish, K., Smith, K., and Guilard, R., Eds.) Vol. 7, pp 339—369, Academic Press, New York.
22. Adak, S., Ghosh, S., Abu-Soud, H. M., and Stuehr, D. J. (1999) *J. Biol. Chem. 274*, 22313—22320.
23. Barrick, D. (1994) *Biochemistry 33*, 6546—6554.
24. DePillis, G. D., Decatur, S. M., Barrick, D., and Boxer, S. G. (1994) *J. Am. Chem. Soc. 116*, 6981—6982.
25. Adachi, S., Nagano, S., Ishimori, K., Watanabe, Y., Morishima, I., Egawa, T., Kitagawa, T., and Makino, R. (1993) *Biochemistry 32*, 241—252.

26. Hirst, J., Wilcox, S. K., Williams, P. A., Blankenship, J., McRee, D. E., and Goodin, D. B. (2001) *Biochemistry 40*, 1265−1273.
27. Zhao, Y., and Marletta, M. A. (1997) *Biochemistry 36*, 15959−15964.
28. Sono, M., Stuehr, D. J., Ikeda-Saito, M., and Dawson, J. H. (1995) *J. Biol. Chem. 270*, 19943−19948.
29. Pond, A. E., Roach, M. P., Thomas, M. R., Boxer, S. G., and Dawson, J. H. (2000) *Inorg. Chem. 39*, 6061−6066.
30. Brandish, P. E., Buechler, W., and Marletta, M. A. (1998) *Biochemistry 37*, 16898−16907.
31. Huff, A. M., Chang, C. K., Cooper, D. K., Smith, K. M., and Dawson, J. H. (1993) *Inorg. Chem. 32*, 1460−1466.
32. *Model J-600 Spectropolarimeter Instruction Manual,* Jasco Corporation Co., Ltd., 14-32, Sennin-cho, Hachioji City, Japan, August 2000.
33. Berka, V., and Tsai, A.-I. (2000) *Biochemistry 39*, 9373−9383.
34. Sono, M., Ledbetter, A. P., McMillan, K., Roman, L. J., Shea, T. M., Masters, B. S. S., and Dawson, J. H. (1999) *Biochemistry 38*, 15853−15862.
35. Mayhew, S. G. (1978) *Eur. J. Biochem. 185*, 535−547.
36. Yoshimura, T., and Ozaki, T. (1984) *Arch. Biochem. Biophys. 229*, 126−135.
37. Hsu, M.-C., and Woody, R. W. (1971) *J. Am. Chem. Soc. 93*, 3515−3525.
38. Vogel, K. M., Hu, S., Spiro, T. G., Dierks, E. A., Yu, A. E., and Burstyn, J. N. (1999) *J. Biol. Inorg. Chem. 4*, 804−813.
39. Decatur, S. M., Franzen, S., DePillis, G. D., Dyer, B., Woodruff, W. H., and Boxer, S. G. (1996) *Biochemistry 35*, 4939−4944.
40. Tomita, T., Ogura, T., Tsuyama, S., Imai, Y., and Kitagawa, T. (1997) *Biochemistry 36*, 10155−10160.
41. Zhao, Y., Hoganson, C., Babcock, G. T., and Marletta, M. A. (1998) *Biochemistry 37*, 12458−12464.
42. Stone, J. R., Sands, R. H., Dunham, W. R., and Marletta, M. A. (1995) *Biochem. Biophys. Res. Commun. 207*, 572−577.
43. Hirst, J., Wilcox, S. K., Ai, J., Moenne-Loccoz, P., Loehr, T. M., and Goodin, D. B. (2001) *Biochemistry 40*, 1274−1283.
44. Stern, J. O., and Peisach, J. (1976) *FEBS Lett. 62*, 364−368.
45. Yoshimura, T. (1983) *Arch. Biochem. Biophys. 220*, 167−178.
46. Suzuki, S., Yoshimura, T., Nakahara, A., Iwasaki, H., Shidara, S., and Matsubara, T. (1987) *Inorg. Chem. 26*, 1006−1008.
47. Migita, C. T., Salerno, J. C., Masters, B. S. S., Martásek, P., McMillan, K., and Ikeda- Saito, M. (1997) *Biochemistry 36*, 10987−10992.
48. Huang, L., Abu-Soud, H. M., Hille, R., and Stuehr, D. J. (1999) *Biochemistry 38*, 1912−1920.
49. O'Keeffe, D. H., Ebel, R. E., and Peterson, J. A. (1978) *J. Biol. Chem. 253*, 3509−3516.
50. Tsubaki, M., Hiwatashi, A., Ichikawa, Y., and Hori, H. (1987) *Biochemistry 26*, 4527−4534.
51. Yumoto, T., Sagami, I., Daff, S., and Shimizu, T. (2000) *J. Inorg. Biochem. 82*, 163−170.
52. Dawson, J. H. (1988) *Science 240*, 433−439.
53. Schilichting, I., Berendzen, J., Chu, K., Stock, A. M., Maves, S. A., Benson, D. E., Sweet, R. M., Ringe, D., Petsko, G. A., and Sligar, S. G. (2000) *Science 287*, 1615−1622.
54. Yoshioka, S., Takahashi, S., Ishimori, K., and Morishima, I. (2000) *J. Inorg. Biochem. 81*, 141−151.
55. Raag, R., and Poulos, T. L. (1989) *Biochemistry 28*, 917−922.
56. Sundarmoorthy, M., Terner, J., and Poulos, T. L. (1995) *Structure 3*, 1367−1377.
57. Suzuki, N., Higuchi, T., Urano, Y., Kikuchi, K., Uekusa, H., Ohashi, Y., Uchida, T., Kitagawa, T., and Nagano, T. (1999) *J. Am. Chem. Soc. 121*, 11571−11572.
58. Ueyama, N., Nishikawa, N., Yamada, Y., Okamura, T., and Nakamura, A. (1996) *J. Am. Chem. Soc. 118*, 12826−12827.
59. Suzuki, N., Higuchi, T., Urano, Y., Kikuchi, K., Uchida, T., Mukai, M., Kitagawa, T., and Nagano, T. (2000) *J. Am. Chem. Soc. 122*, 12059−12060.
60. Pond, A. E., Sono, M., Elenkova, E. A., Goodin, D. B., English, A. M., and Dawson, J. H. (1999) *Biospectroscopy 5*, S42−S52.
61. Traylor, T. G., and Sharma, V. S. (1992) *Biochemistry 31*, 2847−2849.